Egyptian Journal of Petroleum 29 (2020) 203–209

HOSTED BY

Contents lists available at ScienceDirect

Egyptian Journal of Petroleum

journal homepage: www.sciencedirect.com

Full Length Article

Experimental and computational study on electronic and photovoltaic properties of chromen-2-one-based organic dyes used for dye-sensitized solar cells

Elshafie A.M. Gad [a,*], E.M. Kamar [b], Mahmoud A. Mousa [b]

[a] Petrochemicals Dept. Egyptian Petroleum Research Institute, Nasr City 11727, Cairo, Egypt
[b] Chemistry Dept. Faculty of Science, Benha University, Benha, Egypt

ARTICLE INFO

Article history:
Received 21 April 2020
Revised 27 April 2020
Accepted 28 April 2020
Available online 29 May 2020

ABSTRACT

In the present work, three dyes of 6,7-dihydroxy-8-[(*E*)-(4-methoxyphenyl)diazenyl]-4-methyl-2*H*-chromen-2-one, (D1) 6,7-dihydroxy-8-[(*E*)-(4-hydroxyphenyl) diazenyl]-4-methyl-2*H*-chromen-2-one (D2), and 6,7-dihydroxy-4-methyl-8-[(*E*)-(4-methylphenyl) diazenyl]-2*H*-chromen-2-one (D3) were experimentally tested as photosensitizer in solar cell. and a computation study was conducted to explain the efficiency of these compounds as photo-sensitizer in a solar cell. The polarizability (<α >), the anisotropy of the polarizability (<Δα >), ground-state dipole moment (μ) and the first-order hyperpolarizability (β) of the dyes were studied at Density Functional Theory (DFT) using Gaussian 09 and Gauss View v.6.0 based on keywords: "opt freq b3lyp/6-311G++(d,p) guess = mix pop=(nbo, savenbos) geom = connectivity polar = optrot. *Also,* E_{HOMO} (the highest occupied molecular orbital energy), E_{LUMO} (the lowest unoccupied molecular orbital energy), HOMO-LUMO energy gap (ΔE), electron affinity (A), and ionization potential are investigated. The calculation based on the structure modification of the dyes with electron-withdrawing groups (HO-C and CH_3-O-C) and electron repelling group (H_3C-C) based on a push-pull framework of Qumarin was studied. The simulations indicate that the improvement of Qumarin-based dyes can reduce the energy gap and produce a redshift. This structural modification also improves the light-capturing and the electron injection capability, making it excellent in photoelectric conversion efficiency (PCE). This structural modification also improves the light-capturing and the electron injection capability, making it excellent in photoelectric conversion efficiency (PCE).

1. Introduction

Nowadays, major concerns focus on replacing renewable energy instead of petroleum fuels due to its expected depletion. A dye-sensitized solar cell (DSSC) is one of the alternative energies besides wave energy, biofuel, Geothermal power, winds, tidal energy, and Hydrogen gas. DSSC has a great interest due to easy to be fabricated, low cost and ecofriendly. The mechanism of the dye-sensitized solar cell can be summarized in the following steps. First, Absorption of the incident photons by the organic dye. Second, excitation of the organic dye to the excited state then inject the electron to the TiO_2 electrode. Third, the injected electron transferred to the counter electrode through the circuit. Finally, redox reaction (I^-/I_3^-) leads to regenerate of the ground state of the organic dye. E_{HOMO} and E_{LUMO} of the organic dye and the fermi level of the TiO_2 and the redox potential of the mediator (I^-/I_3^-) in the electrolyte are the controlling factors on the efficiency of a DSSC [1]. The most successful structure of organic dyes is based on a dipolar D-π-A push-pull framework; the donor group (D) is responsible for electron donation, linked through a π bridge spacer to the electron-receiving group (A) [2–7]. Computational procedures have been carried out to investigate the relevance of quantum descriptors (Frontier molecular orbital energy and energy gap, natural bond orbitals, dipole moments and hyperpolarizability) to explain the effectiveness of organic dye in a solar cell [8–11]. Fabrication of DSSCs comprises four major parts, 1- Photo-anode made of transparent conducting glass coated with photo-sensitive metal oxide. 2- Photo-sensitizer dye, 3- Redox electrolyte and 4- Counter electrode (Pt) coated with conducting substrate [12–14].

In this study, three dyes were experimentally tested as photo sensitizers in solar cell. These dyes are 6,7-dihydroxy-8-[(E)-

Peer review under responsibility of Egyptian Petroleum Research Institute.
* Corresponding author.
E-mail address: eamgad_99@hotmail.com (E.A.M. Gad).

https://doi.org/10.1016/j.ejpe.2020.04.002

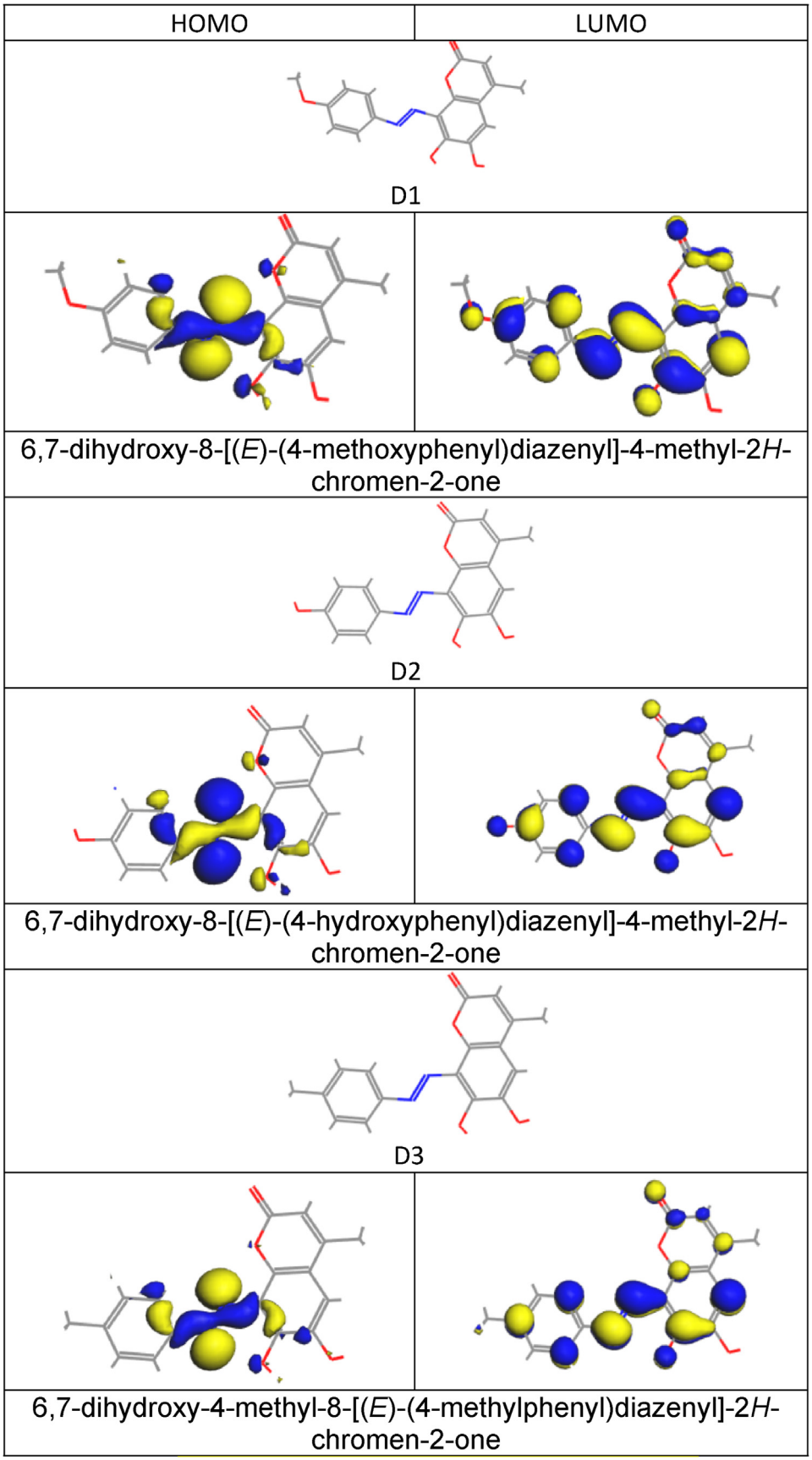

Fig. 1. HOMO and LUMO of the investigated dyes.

Table 1
HOMOs and LUMOs levels of the investigated, redox potential (RP) of I^-/I_3^- and the conduction band CB energy level of TiO2.

	Ref.	D1	D2	D3
LUMO + 2		−1.072	−1.164	−2.002
LUMO + 1		−2.316	−2.356	−3.280
LUMO		−2.919	−2.971	−3.691
HOMO		−4.673	−4.735	−4.950
HOMO-1		−5.123	−5.215	−5.299
HOMO-2		−5.276	−5.315	−5.340
CB	−4.000			
RP	−4.800			
E gap		1.754	1.764	1.259

(4-methoxyphenyl) diazenyl]-4-methyl-2H-chromen-2-one (D1), 6,7-dihydroxy-8-[(E)-(4-hydroxyphenyl) diazenyl]-4-methyl-2H-chromen-2-one (D2) and 6,7-dihydroxy-4-methyl-8-[(E)-(4-methylphenyl)diazenyl]-2H-chromen-2-one (D3).

A computation study based on DFT was conducted to explain the efficiency of these compounds as photo-sensitizer in a solar cell.

2. Experimental

2.1. Materials

FTO conductive glass (sheet resistance: 7 Ω/sq), P25 TiO_2 nanopowder, dyes of 6,7-dihydroxy-8-[(*E*)-(4-methoxyphenyl) diazenyl]-4-methyl-2*H*-chromen-2-one,6,7-dihydroxy-8-[(*E*)-(4-hydroxyphenyl)diazenyl]-4-methyl-2*H*-chromen-2-one, and 6,7-dihydroxy-4-methyl-8-[(*E*)-(4-methyl-8-[E)-(4-methylphenyldiazenyl]-2*H*-chromen-2-one were purchased from Sigma-Aldrich.

2.2. Fabrication of dye-sensitized solar cells (DSSC)

To prepare the working FTO electrodes, the FTO glass was cleaned in a detergent solution with sonication for 20 min and then thoroughly rinsed with deionized (DI) water and ethanol. TiO2 paste was prepared by mixing grounding the TiO_2 powder with distilled water, acetic acid, acetylacetone and polyethylene glycol (PEG). The slurry was ultrasonicated for 40 min, and was placed on a magnetic stirrer at 1100 rpm for 40 min. Ultrasonication and stirring were repeated 5 times to get a consistent viscous slurry of TiO_2. The TiO_2 films were made by spreading TiO2 paste between two Scotch tapes on FTO by the Doctor-blade method. When the paste becomes dry, the two tapes are removed and the TiO_2 mold is fired at 450 °C for 45 min. TheTiO_2-layer with a thickness of 10–12 μm is controlled by the scotch tape. The dye-sensitized TiO_2/FTO photoelectrodes were prepared through soaking the TiO_2/FTO films in a 0.5 mM dye solution (ethanol) for 1 day. The counter electrode is fabricated by the drop-casting method of platinum paste (PT1, Dyesol) onto FTO glass plates. When the platinum paste becomes dry, it is fired at 400 °C for 40 min. After that, two holes are drilled on the counter electrode to facilitate electrolyte injection. The iodide/triiodide (I^-/I_3^-) was used as the electrolyte solution. The resulting counter electrodes and the working TiO_2/FTO electrodes were sealed using a thick Surly. By injecting iodide/triiodide (I^-/I_3^-) electrolyte into the cells through one of the two small holes in the counter electrodes we could prepare TiO_2-based DSSCs with a 20 mm^2 active area.

2.3. Characterizations

UV–Visible absorption spectra of dye solutions were recorded after dilution in ethanol and subsequent ultrasonication using Agilent Cary 60 spectrometer. The film thicknesses of photoanode were examined by a profilometer (model Ambios Technology XP-1). Current-voltage (I-V) characteristics DSSCs are measured under the illumination of AM1.5 condition (100 mW/cm^2) using Xenon lamp (type Oriel 450 W) as a source of light. Collection of I–V data is performed using LabView software. IPCE equipment (type K3100 McScience) is employed to plot the external quantum efficiency as a function of wavelength. Finally, electrochemical measurements were carried out on a Zahner (IM6, Germany).

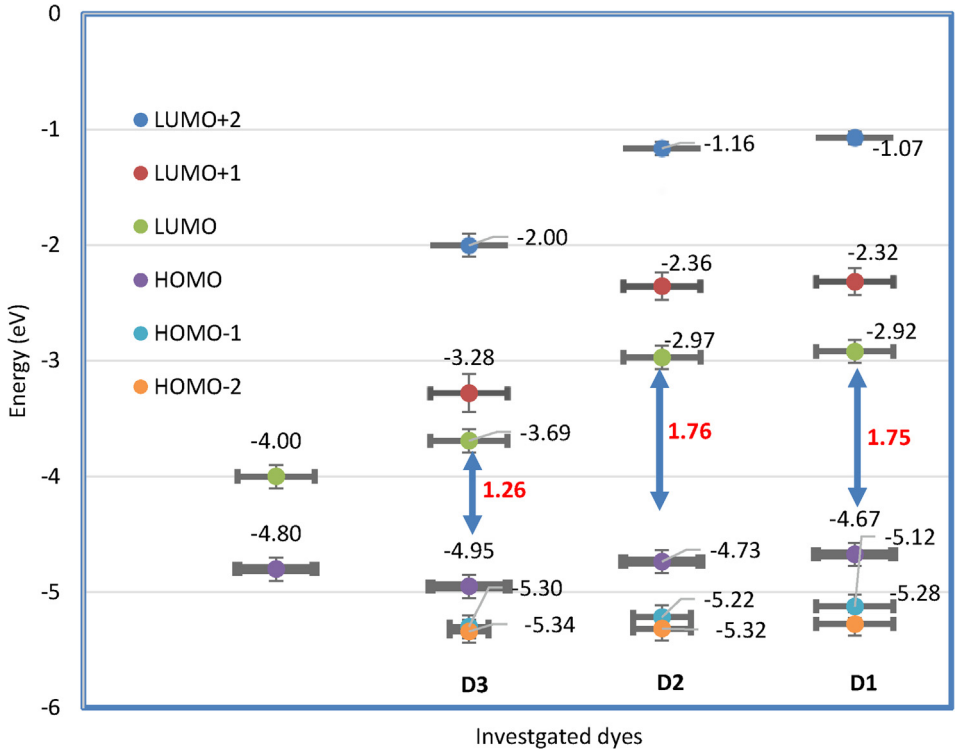

Fig. 2. HOMO and LUMO levels of the investigated dyes compared to redox potential (RP) of I^-/I_3^- (H) and the conduction band (CB) energy levels of TiO_2.

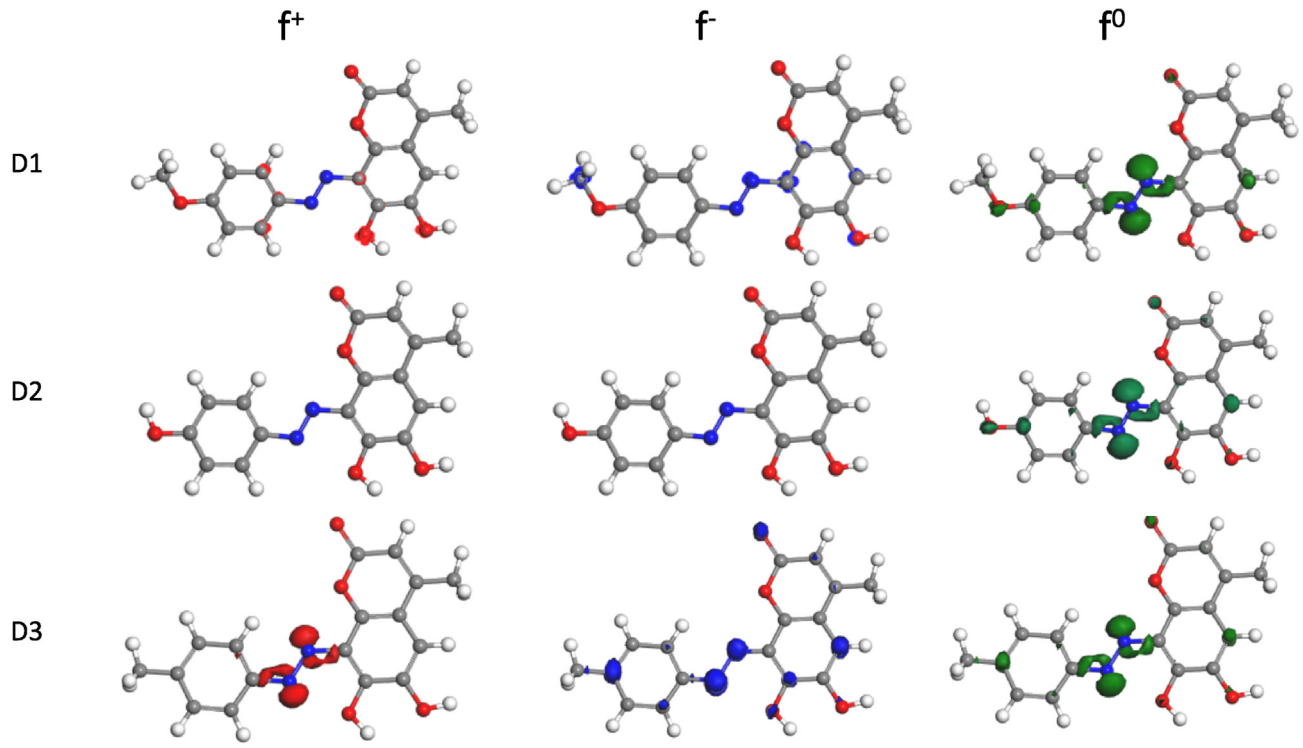

Fig. 3. Graphical representation of Fukui functions (f^+, f^- and f^0) of the investigated dyes.

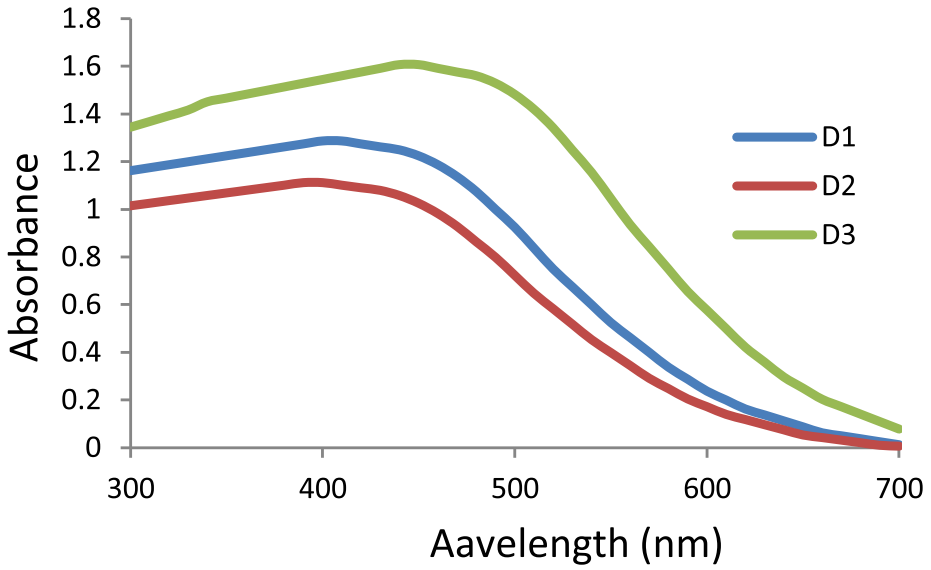

Fig. 4. Experimental Absorption spectra of the investigated dyes.

2.4. Computational methodology

The chemical structures of investigated dyes were designed using ACD/ChemSketch v. 14.01. DMol3 included in Materials Studio v.7.0 (using Local DFT functionals (PWC), GGA-DFT functionals (PBE) and Numerical AO basis sets (DND)) is applied to calculate the Frontier molecular orbitals; E_{HOMO} and E_{LUMO} of the investigated dyes, Fukui' functions (f^+, f^- and f^0) and Natural bonding orbital. The location of the dyes (−8, −9, and −10) on the top of the two layers thickness of TiO_2 and their adsorption energies were determined using Adsorption Locator [15]. The linear, nonlinear optical properties and quantum chemical parameters [16] of the investigated compounds were calculated using Gaussian 09 and Gauss View v.6.0 based on keywords: "opt freq b3lyp/6-311G++(d,p) guess = mix pop=(nbo, savenbos) geom = connectivity polar = opt rot" i.e., dipole moments μ, Polarizability <α> anisotropy of polarizability <Δα> and hyperpolarizability (β).

3. Results and discussion

The geometry optimized structures and Frontier molecular orbitals for HOMO and LUMO levels of the investigated dyes are represented in Fig. 1. The molecular structure is characterized by

D1

		nm	f_osc
85 - 86	H -> L	641	0.000077
83-86	H -2 -> L	486	0.051001
84-86	H -1 -> L	448	0.204105
84-87	H-1 -> L+1	397	0.584468
83-87	H-2 -> L+1	350	0.096989

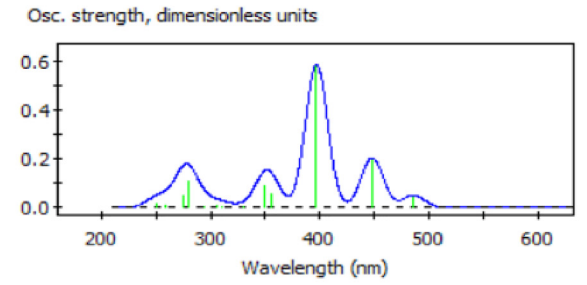

D2

		nm	f_osc
81- 82	H -> L	637	0.000165
79-82	H -2 -> L	486	0.03858
80-82	H -1 -> L	439	0.199191
80-83	H-1 -> L+1	388	0.597882
77-82	H-4 -> L	328	0.004842

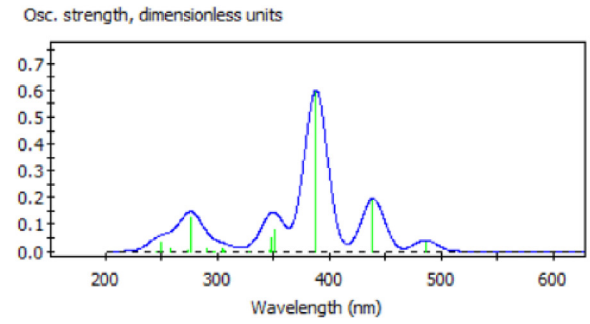

D3

		nm	f_osc
81 - 82	H -> L	874	0.000042
78 - 82	H-3 -> L	681	0.012975
79 - 83	H-2 -> L+1	588	0.050593
78 - 82	H-3 -> L	492	0.649667
78 - 83	H-3 -> L+1	475	0.11949

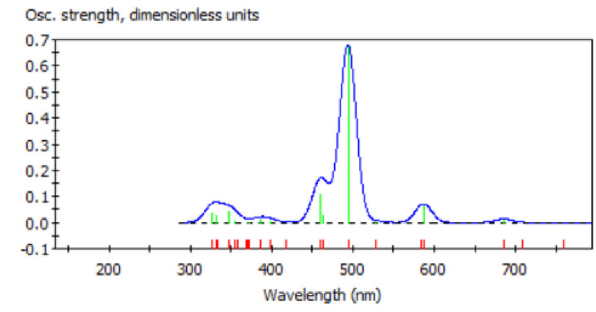

Fig. 5. absorption spectra of the investigated dyes and the corresponding absorption peaks values and oscillator strength according TD-DFT.

Table 2
Dipole moments μ, Polarizability <α> anisotropy of polarizability <Δα> and hyperpolarizability (β).

	Ref.	D1	D2	D3	Urea[a]	THBAP[b]
Total dipole (Debye)	μ	6.0947	6.8981	7.1737	1.373	2.3835
Polarizability (esu)	$<\alpha> \times 10^{-24}$	17.6378	17.3382	17.1412		
Anisotropy (esu)	$<\Delta\alpha> \times 10^{-24}$	20.5929	19.4309	19.9962		
Hyperpolarizability (esu)	$(\beta) \times 10^{-30}$	1.2418	1.5460	1.7400	0.37289	10.0125

[a] Urea[21].
[b] 4-(2,3,4-trihydroxybenzylideneamino) antipyrine[21].

the pull-push framework (D-π -A). D is donating group, π is the conjugated bi-bond and A is an accepting group. Here in the study, the characteristics of the molecules contain carbonyl group C═O which is withdrawing group, azo moiety –N═N– with the conjugated double bonds represent π, The donating groups are CH_3O–, O–, and CH_3– as shown in D1, D2 and Dye10 respectively.

HOMOs are distributed over azo-group and between aromatic moieties. However, LUMOs are distributed over all the molecules. HOMO levels are responsible for electron donation and LUMO levels are liable for electron acceptance. The values of E_{HOMO} AND E_{LUMO} are listed in Table 1. The higher value of E_{HOMO} of the molecule is more susceptible to electron donation. The order of $_{EHOMO}$ of given dyes are D1 (−4.673 eV) > D2 (−4.735 eV) > D3 (−4.950 eV). The Lower value of E_{LUMO} of a molecule is responsible for electron receiving. The order of E_{LUMO} of studied dyes are D3 (−3.691 eV) < D2 (−2.971 < D1 (−2.919 Ev. The difference between E_{LUMO} and E_{HOMO} is the energy gap (Δ E_{gap}) shown in Table 1. The lower bandgap (E_{LUMO}-E_{HOMO}) of D3 indicates a significant effect of intramolecular charge transfer, which would cause an absorption spectrum shifted to red. The reactivity of the investigated dyes according to the values of the energy gap (E_{gap}) is arranged in order of D3 > D1 ≅ D2.

The energy levels of the HOMO and LUMO, as well as the HOMO-LUMO gaps, are drawn in Fig. 2, together with the energy levels of TiO2 semiconductor conduction band (CB = − 4.00 eV) [34] and the redox potential of I^-/I_3^- (RP = − 4.80 eV) [1].

The HOMO of the dye must be below the redox couple (RC) of I^-/I_3^- electrolyte (−4.8 eV) and the LUMO of the dye must be situated above the TiO2 conduction band (−4.0 eV) [17], it is easy to recover electrons from electrolytes. HOMO energy (−4.95 eV) of D3 is

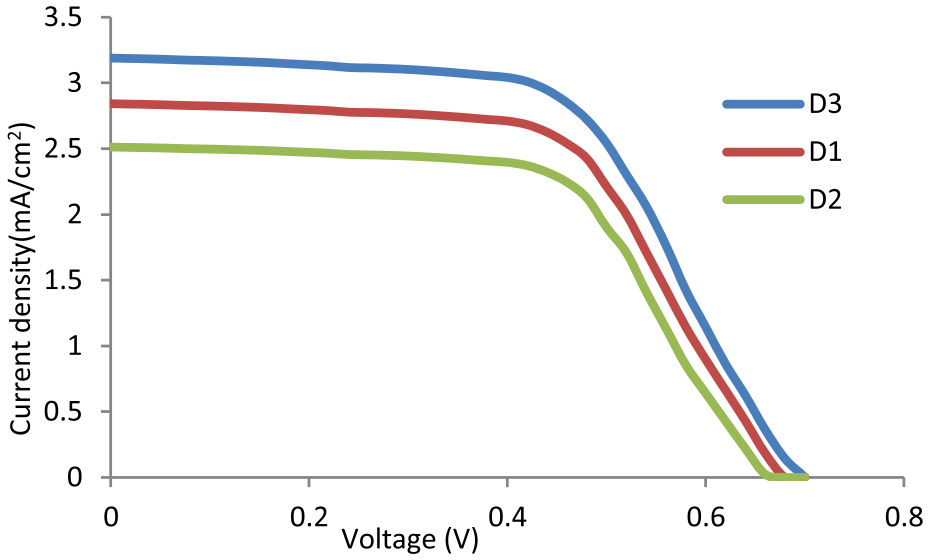

Fig. 6. Experimental J-V curves of the cells made from the investigated dyes and TiO_2 under irradiation intensity of 100 mW/cm^2.

Table 3
DSSC data of the investigated dyes.

Photoelectrode	V_{oc}(V)	J_{sc} (mA/cm^2)	Fill factor	Efficiency%
TiO_2/D3	0.69	3.19	0.65	1.43
TiO_2/D1	0.68	2.84	0.63	1.21
TiO_2/D2	0.66	2.51	0.62	1.02

lower than the RC energy of I^-/I_3^-. However, the studied dyes-9 (−4.67) ≅ D1 (−4.73) approach redox potential energy of TiO_2 (−4.80 eV). It also observed that LUMO energies of these dyes are higher than that of the conduction band (−4.0 eV) that giving enough driving force for excited-state electron injection [18].

Condensed Fukui functions [19] shown in Fig. 3 exhibit a demonstration of the reactive sites in each dyes molecule. The f^+ Fukui function (red clouds), that reflects liability to nucleophilic attack, f^- Fukui function, (blue clouds) that reflects susceptibility to electrophilic attack, and f^0 (green clouds) is accountable for the free radical attack. It is evident that the chemical reactivities of all investigated dyes towards free radical attack is expected, However, reactivities of D1 and D2 towards nucleophilic and electrophilic attack are week. D3 exhibits better relative activity towards the three types of chemical attacks. The susceptible moieties to free radical attacks represent A in A-π-D framework i.e., (CH_3-**C** in D3), (H**O**-**C** in D2**),** and **(**H3C-**O**-**C** in D1) as well as –N═N– π in A-π-D framework that links the conjugation overall molecule in all investigated dyes.

3.1. Absorption spectra

The experimental absorption spectra of the investigated dyes (Fig. 4) in the spectral region from 300 nm to 700 nm. All the dyes show good absorbance in the visible region in the order D3 > D1 > D2 referring to increase the DSSc in the same order.

The absorption spectra of the investigated dyes and the corresponding absorption peaks values and oscillator strength (**f_osc**) as calculates are shown in Fig. 5. According to the attached data in Fig. 5, the main characteristic UV–Vis peaks at excited state are arranged in order D3 (493 nm, f_osc 0.649667) > D1 (397 nm, f_osc 0.584468) > D2 (388 nm, f_osc 0.597882). Thus, the trend in the absorption spectra of the dyes complies with their trend in ΔE_{gap}

3.2. Optical properties

Linear and non-linear optical properties[16], dipole moments μ, Polarizability <α> anisotropy of polarizability <Δα> and hyperpolarizability (β) are determined using Gaussian 09 and Gauss View v.6.0 based on DFT at the basis set b3lyp/6-311G++(d,p) as shown in Table 2. The dipole moment is an indicator of the dipole-dipole intermolecular interactions. However, Non-linear optical (NLO) properties represent the intramolecular charge delocalization in A-π-D organic dye sensitizers [20]. Molecules of higher dipole moment have stronger intermolecular interactions. The lower energy gap, the longer wavelength of UV–visible absorption that leads to redshift. Hence, an increase in molecular hyperpolarizability is observed. i.e., D3 has a lower energy gap as compared to D2 and D1. On the contrary, D3 has higher value of the first hyperpolarizability that indicate to a higher rate of intermolecular charge transfer. This can be accounted that A moiety (CH_3-**C**) in D3 electron repelling group via σ bond. However, Oxygen in (H**O**-**C** in D2), and **(**H3C-**O**-**C** in D1) plays dual function electron withdrawing via σ bond due to electronegativity and electron delocalization of lone pair via π. So, D3 pronounced better optical properties. According to the data of calculated hyperpolarizability of the investigated dyes, it is observed that the obtained values are higher than the corresponding value of urea [21] and smaller than that of 4-(2,3,4-trihydroxybenzylideneaino) antipyrine [22]. These data imply that the studied dyes are good candidate of NLO materials

The experimental results (J-V plots) of the DSSCs with D1, D2, and D3 as the active dyes are shown in Fig. 6. The DSSCs revealed higher current density and larger area under the J-V curve in the order D3 > D1 > D2. The photovoltaic parameters of the tandem cells: short circuit current density (JSC), open-circuit voltage (VOC), conversion efficiency (η) and fill factor (FF), are summarized in Table 3. It shows that the highest conversion efficiency is

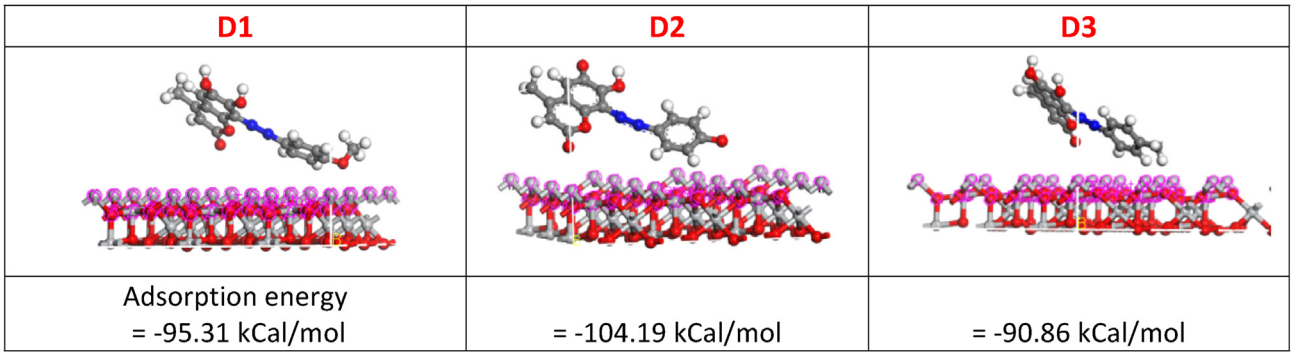

Fig. 7. Chemical structures and binding energies of the investigated dyes adsorbed on the top of the surface of TiO_2.

about 1.43% for tandem parallel cell containing D3 dye with JSC = 3. 19 mA/cm^2, VOC = 0.69 V and FF = 0.65.

3.3. Adsorption of investigated dyes on TiO_2

The importance of the adsorption of the DSSC on TiO_2 could improve the efficiency of dye-sensitized solar cells [23]. The determined adsorption energy of the studied dyes and their location on the top of the layer of TiO_2 are illustrated in Fig. 7. Graphical representation of Fukui functions shown in Fig. 3, it is observed that CH3-O-C, H-O-C and CH3-C for D1, D2 and D3 respectively are susceptible to the free radical attack. Thus, the optimum situation obtained for the dyes could help in the electron transfer to the photoanode.

4. Conclusion

In this study, the DFT and TD-DFT methods were used to calculate the properties of the ground and excited states for D1, D2, and D3. The calculated results show that D3 has the highest HOMO energy compared to D2 and D1, resulting in the smallest energy gap. Smaller energy gaps favor the red-shifted absorption; so, it has the most pronounced red-shifted absorption and the highest molar extinction coefficient, which results in more effective absorption of sunlight. This is consistent with the experimental results that D3 has the highest *J*SC and *V*OC. The calculated results for the design molecules show that the overall effect is improved to some extent. For different groups, by introducing the $-CH_3$ group, the LUMO energy, and energy gap can be reduced, leading to an obvious redshifted absorption. Chemical reactivity parameters and β were significantly improved.

Declaration of Competing Interest

The authors declare that they have no known competing financial interests or personal relationships that could have appeared to influence the work reported in this paper.

References

[1] K. Sharma, V. Sharma, S.S. Sharma, Dye-sensitized solar cells: fundamentals and current status, Nanoscale Res. Lett. 13 (2018) 1–47.
[2] M. Pastore, E. Mosconi, F. De Angelis, M. Grätzel, A computational investigation of organic dyes for dye-sensitized solar cells: Benchmark, strategies, and open issues, J. Phys. Chem. C 114 (15) (2010) 7205–7212.
[3] H. Wang, Q. Liu, D. Liu, R. Su, J. Liu, Y. Li, Computational prediction of electronic and photovoltaic properties of anthracene-based organic dyes for dye-sensitized solar cells, Int. J. Photoenergy 2018 (2018) 1–17.
[4] M.A.M. Rashid, D. Hayati, K. Kwak, J. Hong, Computational investigation of tuning the electron-donating ability in metal-free organic dyes featuring an azobenzene spacer for dye-sensitized solar cells, Nanomaterials 9 (1) (2019) 1–14.
[5] T. Delgado-Montiel, R. Soto-Rojo, J. Baldenebro-López*, D.I. Glossman-Mitnik, Theoretical study of the effect of different π bridges including an azomethine group in triphenylamine-based dye for dye-sensitized solar cells, Molecules. 24(21) 3897, 1–16, 2019.
[6] A.N.B. Zulkifili, T. Kento, M. Daiki, A. Fujiki, The basic research on the dye-sensitized solar cells (DSSC), J. Clean Energy Technol. 3 (5) (2015) 382–387.
[7] M. Pastore, First principle modelling of materials and processes in dye-sensitized photoanodes for solar energy and solar fuels, Computation 5 (1) (2017) 1–22.
[8] U. Mehmood, S.U. Rahman, K. Harrabi, I.A. Hussein, B.V.S. Reddy, Recent advances in dye sensitized solar cells, Adv. Mater. Sci. Eng. 2014 (2014) 1–12.
[9] M. Bourass et al., Theoretical studies by using the DFT and TD-DFT of the effect of the bridge formed of thienopyrazine in solar cells, J. Mater. Environ. Sci. 6 (6) (2015) 1542–1553.
[10] P. Ren, Y. Li, Y. Zhang, H. Wang, Q. Wang, Photoelectric properties of DSSCs sensitized by phloxine B and bromophenol blue, Int. J. Photoenergy 2016 (2016) 1–11.
[11] R.A. Toor, M.H. Sayyad, S.A.A. Shah, N. Nasr, F. Ijaz, M.A. Munawar, Synthesis, computational study and characterization of a 3-{[2,3-diphenylquinoxalin-6-yl]diazenyl}-4-hydroxy-2H-chromen-2- one azo dye for dye-sensitized solar cell applications, J. Comput. Electron. 17 (2) (2018) 821–829.
[12] R. Ali, N. Nayan, Fabrication and analysis of dye-sensitized solar cell using natural dye extracted from dragon fruit, Cell, pp. 55–62, 2010.
[13] D. Sinha, D. De, D. Goswami, A. Ayaz, Fabrication of DSSC with nanostructured ZnO photo anode and natural dye sensitizer, Mater. Today Proc. 5 (1) (2018) 2056–2063.
[14] G.J. Wang, G.Y. Chen, M.W. Lee, Fabrication of dye-sensitized solar cells with a 3D nanostructured electrode, Int. J. Photoenergy 2010 (2010) 1–7.
[15] M. Abdallah, E.A.M. Gad, J.H. Al-Fahemi, M. Sobhi, Experimental and theoretical investigation by DFT on the some azole antifungal drugs as green corrosion inhibitors for aluminum in 1.0M HCl, Prot. Met. Phys. Chem. Surfaces 54 (3) (2018) 503–512.
[16] A. Eşme, S. Güneşdoğdu Sağdinç, The linear, nonlinear optical properties and quantum chemical parameters of some sudan dyes, BAÜ Fen Bil. Enst. Derg. Cilt 16 (1) (2014) 47–75.
[17] R. Li, X. Lv, D. Shi, D. Zhou, Y. Cheng, G. Zhang, P. Wang, Dye-sensitized solar cells based on organic sensitizers with different conjugated linkers: furan, bifuran, thiophene, bithiophene, selenophene, and biselenophene, J. Phys. Chem. C, vol. 113, no. 17, pp. 7469–7479, 2009.
[18] S. Meng, E. Kaxiras, Electron and hole dynamics in dye-sensitized solar cells: influencing factors and systematic trends, Nano Lett. 10 (4) (2010) 1238–1247.
[19] J. Oláh, C. Van Alsenoy, A.B. Sannigrahi, Condensed Fukui functions derived from stockholder charges: assessment of their performance as local reactivity descriptors, J. Phys. Chem. A 106 (15) (2002) 3885–3890.
[20] D.S. Patil, K.C. Avhad, N. Sekar, Linear correlation between DSSC efficiency, intramolecular charge transfer characteristics, and NLO properties – DFT approach, Comput. Theor. Chem. 1138 (2018) 75–83.
[21] Y.X. Sun et al., Experimental and density functional studies on 4-(3,4-dihydroxybenzylideneamino)antipyrine, and 4-(2,3,4-trihydroxybenzylideneamino) antipyrine, J. Mol. Struct. Theochem. 904 (1–3) (2009) 74–82.
[22] X.H. Li, Z. Mei, X.Z. Zhang, Computational study of the vibrational spectroscopic studies, natural bond orbital, frontier molecular orbital and second-order non-linear optical properties of acetophenone thiosemicarbazone molecule, Spectrochim. Acta – Part A Mol. Biomol. Spectrosc. 118 (2014) 543–551.
[23] M.K. Hossain, M.F. Pervez, M.J. Uddin, S. Tayyaba, M.N.H. Mia, M.S. Bashar, M.K. H. Jewel, M.A.S. Haque, M.A. Hakim, M.A. Khan, Influence of natural dye adsorption on the structural, morphological and optical properties of TiO2 based photoanode of dye-sensitized solar cell, Mater. Sci. Pol. 36 (1) (2018) 93–101.